

# Control of Strong Motion by the Upper 30 Meters

by John G. Anderson, Yajie Lee, Yuehua Zeng, and Steven Day

**Abstract** Local site effects have an enormous influence on the character of ground motions. Currently, soil categories and site factors used in building codes for seismic design are generally based on, or at least correlated with, the seismic velocity of the surface layer. We note, however, that the upper 30 m (a typical depth of investigation) would almost never represent more than 1% of the distance from the source; 0.1% to 0.2% would be more typical of situations where motion is damaging. We investigate the influence of this thin skin on the high-frequency properties of seismograms. We examine properties of seismograms consisting of vertically propagating  $S$  waves through an arbitrarily complex stack of flat, solid, elastic layers, where the properties of the lowermost layer (taken at 5 km depth) and a surface layer (thickness 30 m) are constrained. Input at the bottom of the stack is an impulse. We find that the character of the seismograms, and the peak spectral frequencies, are strongly influenced by the properties of the intervening layers. However, for infinite  $Q$ , the integral of amplitude squared at the surface (which determines energy if the input and output are regarded as velocity, or Arias intensity if the input and output are regarded as acceleration) is independent of the intervening layers. Also, the peak amplitude of the seismogram at the surface is relatively independent of the intervening properties. For finite, frequency-independent  $Q$ , the integral of amplitude squared and peak amplitude decrease as  $t^*$  increases. There is some scatter that depends on the intervening layers, but it is surprisingly small.

These calculations suggest that the surficial geology has a greater influence on ground motions than might be expected based on its thickness alone. They suggest that variable influences of  $Q$  along the entire path have a comparable importance for predictions of ground motions. Finally, they suggest that detailed characterization of deeper velocity structure in regions where a 1D model is appropriate gives only a limited amount of added information. Based on our 1D numerical results, we propose a new method to characterize these properties as site factors that could be used in building codes. Full three-dimensional synthetics are tested and give a similar conclusion.

## Introduction

In engineering site investigation, 30 m is a typical depth of borings and detailed site characterizations. Therefore, most of the site-effect studies in earthquake ground motions are based on the properties in the upper 30 m. For instance, Boore *et al.* (1993, 1994) based their regressions for ground motions on average shear velocity in the upper 30 m. Borchardt (1992, 1994) and Martin and Dobry (1994) recommended that design of structures be based on these properties.

From the seismological perspective, the upper 30 m is an extremely thin skin. For an earthquake at a depth of 10 to 15 km, it represents, at most, 0.3% of the path. Even at 10 Hz, it is less than the wavelength of a shear wave unless the velocity is quite low, less than 0.3 km/sec. From this

perspective, even though it is the section closest to the structure, it is not obvious that it should play a critical role. Surprisingly, we have found few systematic studies, either theoretical or empirical, comparing the contributions of the upper 30 m with the rest of the path.

Two strong-motion records from the 1989 Loma Prieta earthquake provide a good example. Figure 1 shows the locations of two strong-motion stations, ASH (Agnews State Hospital) and HAL (Halls Valley), and the vertical projection of the rupture zone in the 1989 Loma Prieta earthquake. Both stations are about the same distance from the rupture zone: From Figure 1, ASH is 40 km from the epicenter and 24 km from the fault, while HAL is 37 km from the epicenter and 30 km from the fault. The shear velocities of the upper 30

Loma Prieta Earthquake Oct 17, 1989

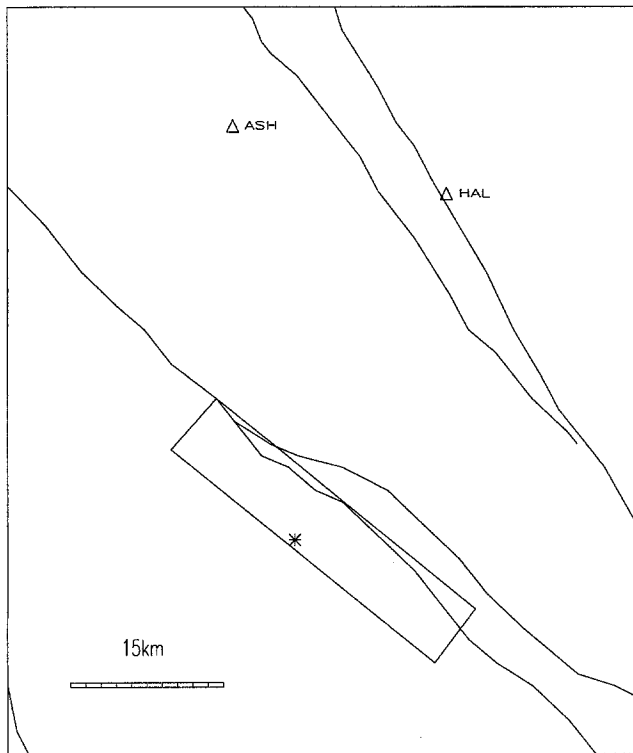


Figure 1. Map showing locations of stations ASH and HAL, relative to the surface projection of the rupture of the 1989 Loma Prieta earthquake, after Zeng *et al.* (1993).

m under these two stations are 264 and 265 m/sec (Thiel and Schneider, 1993), respectively. However, the ground motions shown in Figure 2 at these two stations have significant differences. The accelerograms at station ASH have more high-frequency energy than those at station HAL. Between about 0.8 and 2 Hz, however, they are comparable. Differences at lower frequencies could result from the radiation pattern and source directivity. Following the method of Anderson and Hough (1984) to quantify the high-frequency spectral falloff, in the frequency range from 1.0 to 10.0 Hz, we found  $\kappa = 0.064$  sec at ASH, and  $\kappa = 0.095$  sec at HAL. The similar conditions in the upper 30 m undoubtedly influence the general amplitudes and characteristics of their accelerograms, but other parts of the path then would be a likely cause of the significant differences.

This article addresses the relative importance of effects of the upper 30 m, compared to the velocity structure below, on vertically propagating  $S$  waves in a horizontally layered earth model. We take the perspective that we can draw upon seismological information for reasonably good control of the velocity structure and  $Q$  value at 5 km depth but that the structure is completely unknown, and any reasonable structure is possible between 5 km and 30 m below the surface. The 5-km depth is arbitrarily chosen, and the results are independent of exactly where this lower interface is located.

We examine numerical results for both simple and very irregular 1D velocity models. Also, we change the properties in the upper 30 m to examine their influence on the ground motions. We also show preliminary 3D simulations using the composite source model approach (Zeng *et al.*, 1994; Yu, 1994) that indicate that the results from the 1D vertical propagation model are similar to those for more realistic situations.

## Theoretical Results

Figure 3 illustrates the model that is examined in this article. The Earth is modeled as a series of  $N$  horizontal layers overlying a uniform half-space. The  $i$ th layer is homogeneous and isotropic, with thickness  $h_i$ , density  $\rho_i$ , shear velocity  $\beta_i$ , and frequency-independent spatial attenuation quality factor  $Q_i$ . The model is excited by a planar  $S$  wave, propagating vertically from within the half-space. Thus the wave is purely  $SH$  in polarization. By introducing discontinuities in material properties and consequent reflection and transmission coefficients, this model is more general than the one considered by Joyner *et al.* (1981). They found that the nonresonant amplification produced by waves propagating through nonattenuating materials of gradually changing velocity is, in our notation,  $\sqrt{\rho_N + 1}\beta_N + 1/\rho_1\beta_1$ . This amplification, of course, would be doubled when the effect of the free surface is included. Day (1996) used the general layered model to examine the response of a perfectly elastic half-space to an incident  $SH$  wave. He found that certain spectral averages of the site amplification function, taken over bandwidth  $\Delta f$ , depended only on the elastic structure down to a two-way travel-time depth of  $1/\Delta f$ . Both of these results are only valid when  $Q$  is infinite. Still, they suggest a surprisingly strong influence of the shallowest part of the path, and the motivated this numerical study.

Transfer functions, and synthetic seismograms at the surface of the layered half-space, are computed using propagator matrices based on the method of Luco and Apsel (1983). We compare the surface seismogram with the input in two ways. First, we find the ratio of peak amplitude at the surface to peak amplitude of the input. This ratio might generally be expected to be greater than 2, since the free-surface effect contributes. However, when attenuation is included, it does not need to be this large. Second, we examine the integral of amplitude squared:

$$A = \int_0^{\infty} s^2(t) dt$$

in which  $s(t)$  is the seismogram at the surface. The ratio  $A_{\text{surface}}/A_{\text{input}}$  is the quantity examined by Day (1996). When the impulse and, consequently,  $s(t)$ , is regarded as velocity,  $A$  is proportional to the energy in the wave field. When the seismogram is an accelerogram,  $A$  is proportional to the Arias intensity (Arias, 1970), which is  $(\pi/2g) A$ , where  $g$  is

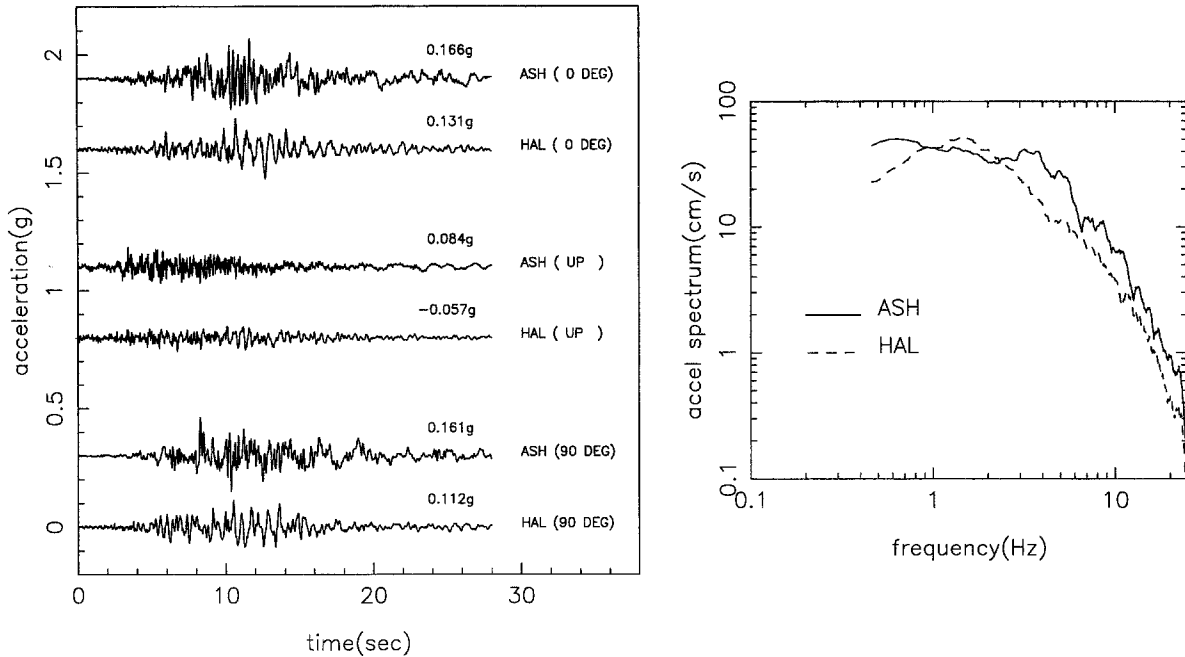


Figure 2. Accelerograms and corresponding Fourier spectra from stations ASH and HAL in the 1989 Loma Prieta earthquake. Peak motions are indicated. Fourier spectra are the average of the two horizontal components and smoothed so that the RMS amplitude is not affected.

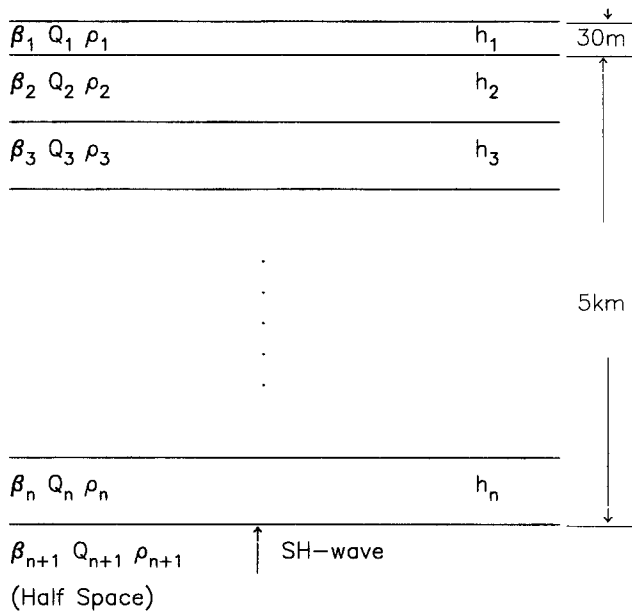


Figure 3. The model used in our calculations.

the acceleration of gravity. Regarding the input as acceleration,  $A$  is also closely related to the RMS acceleration:  $a_{rms} = \text{RMS}\{s(t)\} = \sqrt{A/T}$ , where  $T$  is the duration of the record (e.g., Hanks, 1979; Hanks and McGuire, 1981). Since peak acceleration is generally proportional to RMS acceleration (e.g., Hanks and McGuire, 1981), the peak amplitudes and the squared integral  $A$  are expected to show similar trends.

The ratio of peak amplitudes or the integrals of amplitude squared at the surface to the input are the same regardless of whether this input is considered to be acceleration, velocity, or displacement. However, the spectrum of the input is more like the typical spectrum of strong-motion acceleration (e.g., Brune, 1970; Hanks, 1979) than the spectrum of strong-motion velocity or displacement. Thus, for applications to strong-motion seismology, it is most appropriate to think of the input as an impulse in acceleration.

This article defines the "stratified medium index" (SMI) as  $\text{SMI} = (A_{\text{surface}}/4A_{\text{input}})$ , for notation to describe changes in  $A$  as a function of differences in the velocity model. With the factor of 4 in the denominator, SMI equals unity at the surface of a uniform, nonattenuating half-space. Thus, it could simulate an experiment that finds the ratio of Arias intensity at an arbitrary site to the Arias intensity on "rock." Except for the factor of 4 in the denominator, it is the square of the RMS amplification, as defined by Day (1996). The terminology is analogous to terminology used by Sanchez-Sesma *et al.* (1986), who defined the topographical effects index (TEI) as the ratio of the Arias intensity at a site affected by topography to a site in the free field. Both of these indexes could be special cases of a "site effects index (SEI)," which gives the Arias intensity ratio to a reference rock site.

It is convenient to define  $t^*$  in the traditional seismological sense as an average property of the attenuation in the layered stack. Specifically,

$$t^* = \sum_{i=1}^N \frac{h_i}{Q_i \beta_i}$$

In the frequency domain, the total effect of attenuation on a ray that passes directly through the stack is to reduce the amplitude by  $e^{-\pi f t^*}$ . This amplitude reduction does not account for frequency-independent transmission coefficients at the layer boundaries. Further, waves that take a less direct path, due to multiple reflections along the way, will have their spectra modified by a different factor, accounting for multiple passages through various layers. Still, we examine this parameter to evaluate if it is a useful parameter to describe the average effects of attenuation.

### Numerical Results

Results based on vertical *SH*-wave propagation through the model in Figure 3 are shown in Figures 4 through 10. Our input for these runs is an impulsive pulse—in other words, a time series with one point only that is different from zero. The pulse is input as a signal traveling vertically in layer  $n + 1$  from below the interface; the response of the interface at a 5-km depth depends on the contrast with the layer above.

Initially, the properties of the surface layer are fixed as follows:  $h_1 = 30$  m,  $\rho_1 = 1.7$  g/cm<sup>3</sup>,  $\beta_1 = 400$  m/sec, and  $Q_1 = 30$ . In addition, the properties of the basement are fixed as  $z_{N+1} = 5000$  m,  $\rho_{N+1} = 2.8$  g/cm<sup>3</sup>,  $\beta_{N+1} = 3640$  m/sec, and  $Q_{N+1} = 1000$ . Intervening layers are varied in a number of ways. The two-way travel time through the upper 30 m is 0.15 sec in this model, so Day (1996) indicates that spectral averages over a bandwidth of 6.7 Hz would be independent of the deeper layers if  $Q$  were infinite.

$Q$  values used in our numerical models are chosen to be

similar to real situations. Several studies have investigated the attenuation effects of the near surface on shear waves. For instance, Hauksson *et al.* (1987) estimated that  $Q$  for shear waves averages 25 between 420 m and the surface in Pliocene–Pleistocene sediments in the Los Angeles basin. At Vinyard Canyon, near Parkfield, Gibbs and Roth (1989) obtained  $Q = 4$  in the 57- to 102-m depth interval of a 195-m borehole. Fletcher *et al.* (1990) studied two granitic sites near Anza, California. In the upper 50 m, they found  $Q = 8$  at one and 11 at the other. Gibbs *et al.* (1994) obtained a mean value of  $Q$  close to 10 over the depth range 10 to 115 m in Santa Clara Valley, California. All these studies indicate very low  $Q$  values near the surface. In our numerical calculations, we assign a  $Q$  value to the surface layer that is reasonably consistent with these studies and assume that it generally increases as velocity increases. The  $Q$  values assigned to intermediate layers are between those of the surficial layer and the basement.

The simplest case is for two layers over the half-space ( $N = 2$ ). Figure 4 shows an example seismogram and spectrum for this case, in which  $\beta_2 = 1500$  m/sec,  $Q_2 = 150$ , and  $\rho_2 = 2.2$  g/cm<sup>3</sup>. On the left, the solid line gives the complete seismogram at the base of the stack, at  $z = 5$  km, and the dashed line shows the seismogram at the surface. The input *S* wave is an impulse arriving at the interface at  $t = 1.0$  sec. The pulse arrives at the surface about 3.5 sec later and causes the surface layer to resonate. Some of the energy is transmitted back into layer 2, first arriving at the lower interface another 3.5 sec later. The high-frequency reverberation at the lower interface is caused by a series of pulses sequentially leaving layer 1 after a series of surface

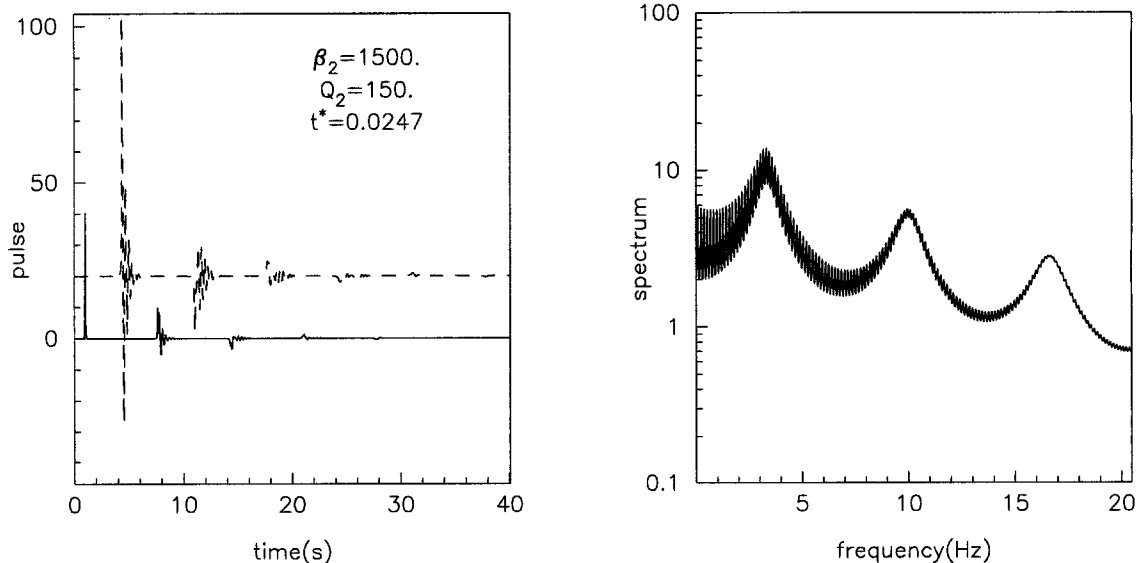


Figure 4. Sample calculations for two layers. Seismograms from the base (solid) and surface (dashed) are shown at the left. The seismogram at the base shows the vertically propagating impulse used for all calculations arriving at  $t = 1.0$  sec, followed by reflections from the surface. Properties of the model are given in the figure. The Fourier spectrum of the seismogram at the surface is given at the right.

reflections. Some of this energy is, in turn, reflected back, causing the second packet of energy to arrive at the surface starting at about 11 sec. The Fourier amplitude spectrum on the right consists primarily of the superposition of two features. Most conspicuous are strong peaks at 3.3, 10, and 16.7 Hz caused by the reverberations in the thin shallow layer. This causes the “ringy” character of the signal. The closely spaced peaks and troughs superimposed on this major trend are caused by the “resonance” of the thick middle layer, with a fundamental frequency of about 0.08 Hz (period of about 13 sec). This resonance is not seen in the seismograms in Figure 4, since the spectral content of the source emphasizes much higher frequencies.

Figure 5 shows some generalized results for two layers over a half-space. The right side shows the peak amplitude ratio of the seismogram on the surface to the amplitude of the input for a series of computations in which  $\beta_2$  and  $Q_2$  are taken to be variables. On the left, it shows SMI for the same combinations of  $\beta_2$  and  $Q_2$ . The dashed line represents the case with very high  $Q_1$  ( $= 1000$ ) in the surface layer. For the highest values of  $Q_1$  and  $Q_2$ , SMI becomes nearly independent of  $\beta_2$ , as predicted by Day (1996). Peak amplitude ratios are not completely independent of  $\beta_2$ . In the limits of the intermediate layer being the same as the half-space or the upper 30 m, there is effectively only one layer over the half-space, and because it is much weaker, the transmission coefficient approaches 2.0. With very high  $Q$ , the amplitudes are doubled again at the free surface, resulting in amplifi-

cation of the peak amplitude by about a factor of 4.0. Where layer 2 has an intermediate velocity, there are two transmission coefficients, and their product is greater than 2.0, causing the peak in the amplification function when  $Q$  is high. As obtained from the equation from Joyner *et al.* (1981) that was cited earlier, the limiting amplification for this case, which would be approximated by a large number of layers each with a small velocity contrast, is 7.7. As  $Q_2$  decreases, both the SMI and the peak amplitudes decrease.

These simple calculations indicate that the attenuation properties along the entire path of wave propagation play a significant role on ground-motion predictions. In fact, they indicate that the attenuation properties may be more important than the velocity in the intermediate layer in affecting peak amplitude and RMS amplitudes at the surface.

We now move to more complicated cases. Figure 6 plots three of a class of models with both velocity and  $Q$  values monotonically increasing with increasing depth. Figure 7 shows a very irregular model in which velocities in intermediate layers are chosen at random within limits. Low-velocity layers are included in these irregular models, and there is no definite relation between the velocity and the  $Q$  values.

We first examine the correlation between  $t^*$  and the character of the seismogram in terms of SMI and peak amplitudes. Figure 8 shows the results obtained from these models. The dashed line is for models whose velocity and  $Q$  values increase monotonically with depth, and the stars

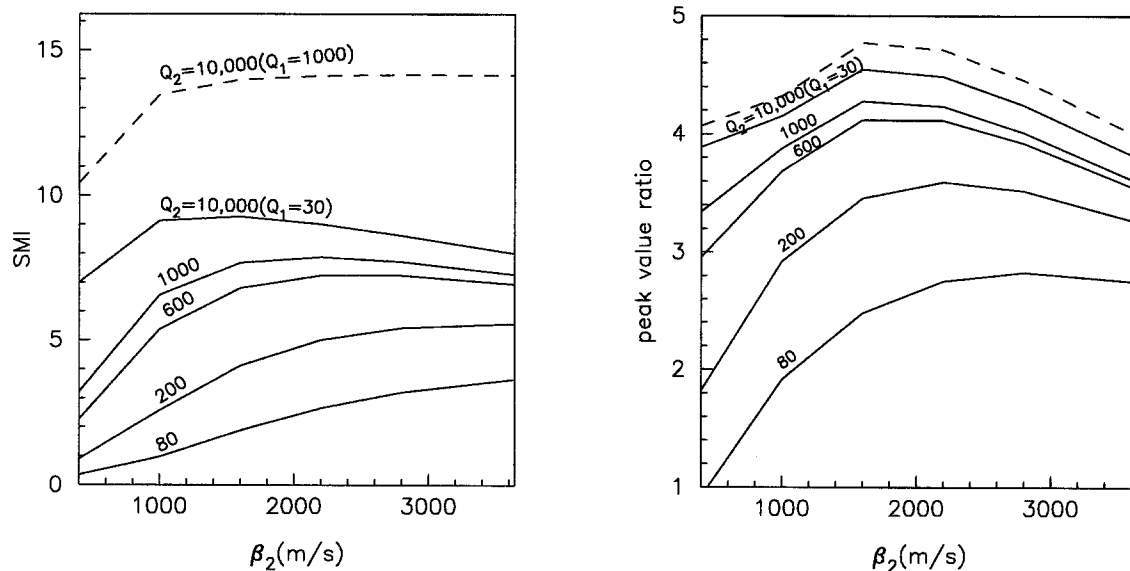


Figure 5. Peak amplitude ratios and the stratified medium index (SMI) for models consisting of two layers over a half-space, as a function of velocity in the intermediate layer. Each curve corresponds to a different value of  $Q$  in the intermediate layer, with values as given. All curves except for the dashed ones use  $\beta_1 = 400$  m/sec and  $Q_1 = 30$ ; the dashed curves increase  $Q_1$  to 1000. SMI is the ratio of the integral of amplitude squared at the surface to the input at 5 km in depth. Ratios are divided by 4.0 to compensate for amplitude doubling at the free surface and give SMI = 1.0 on a uniform, nonattenuating half-space.

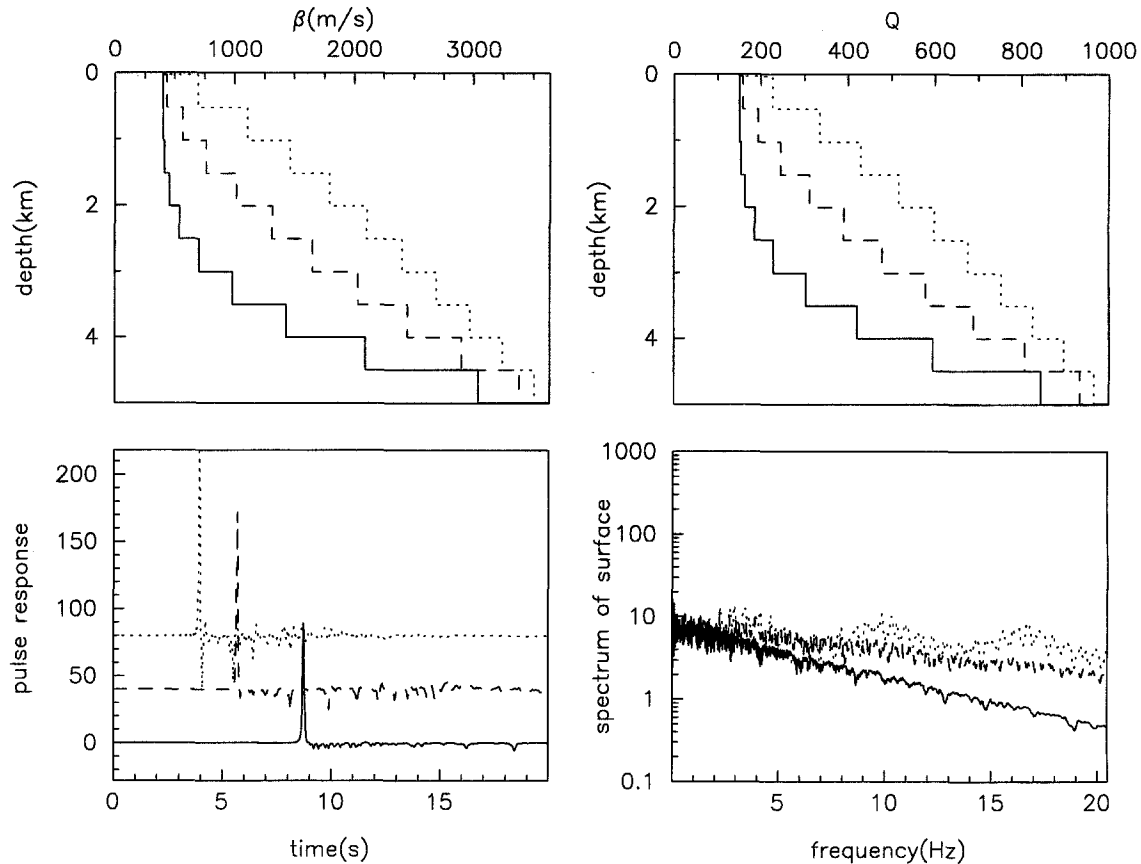


Figure 6. Velocity (top left) and  $Q$  (top right) models with monotonic increases between the surface and 5 km in depth, and corresponding seismograms (bottom left) and spectra (bottom right). Two of the seismograms are offset from zero for clarity of presentation. To generate a velocity model, we found a continuous function of the form  $\beta(z) = c_1 + c_2 z^n$  that matched the velocity at the base of the layer 1 and the top of the half-space. The velocity of each layer is the value of this function at the midpoint of the layer.  $Q$  models are found the same way, and use the same value of  $n$  as the shear velocity model. Different members of this class are obtained using different values of  $n$  in the range  $0.25 \leq n \leq 2.0$ .

represent the results obtained from the irregular models. The SMI decays approximately exponentially on  $t^*$  with some scatter, depending on the intervening layers, reaching an upper limit when velocity and  $Q$  values increase monotonically with depth (the dash line). A similar result occurs for the peak amplitudes. From these calculations, we conclude that for a specific surficial site condition, both SMI and peak amplitude of ground motions are reasonably well correlated with  $t^*$ , which is able to describe the attenuation properties of the underlying structures.

Another important feature of Figure 8 is the total amount of scatter in the models with irregular velocity profiles. In generating the random velocity profiles, we allowed the velocities to deviate from the mean by up to 30% of the mean. This is a very large range compared to what we believe to be most realistic, which is a deviation of 5% to 10%. Still, the scatter in both SMI and the peak value ratio is generally less than about 50%. Since the amount of scatter increases with an increased amplitude of randomness in the

velocity profile, these plots suggest that the total influence of the details of the velocity profile is quite small compared to the influence of  $t^*$ . This extends the conclusions found by Day (1996), indicating that  $t^*$  and the elastic structure at the top of the stack, to surprisingly good precision, control the SMI and the peak motion. As in Day (1996), these are largely independent of the deeper elastic structure.

We next investigate the influence of the near-surface properties simultaneously with those of underlying layers. We fix the shear velocity of the upper 30 m to the boundary values for site classification proposed by Martin and Dobry (1994) and change the properties below it. There are minor differences in the cutoff velocities between Martin and Dobry (1994) and other articles using this approach (Boore *et al.*, 1993; Borchardt, 1992, 1994). We then repeat the same calculations as before but use only those models with velocity and  $Q$  increasing monotonically with depth because of the upper-limit properties mentioned above. Results obtained are shown in Figure 9. Zones  $A_0$ , A, B, C, and D are

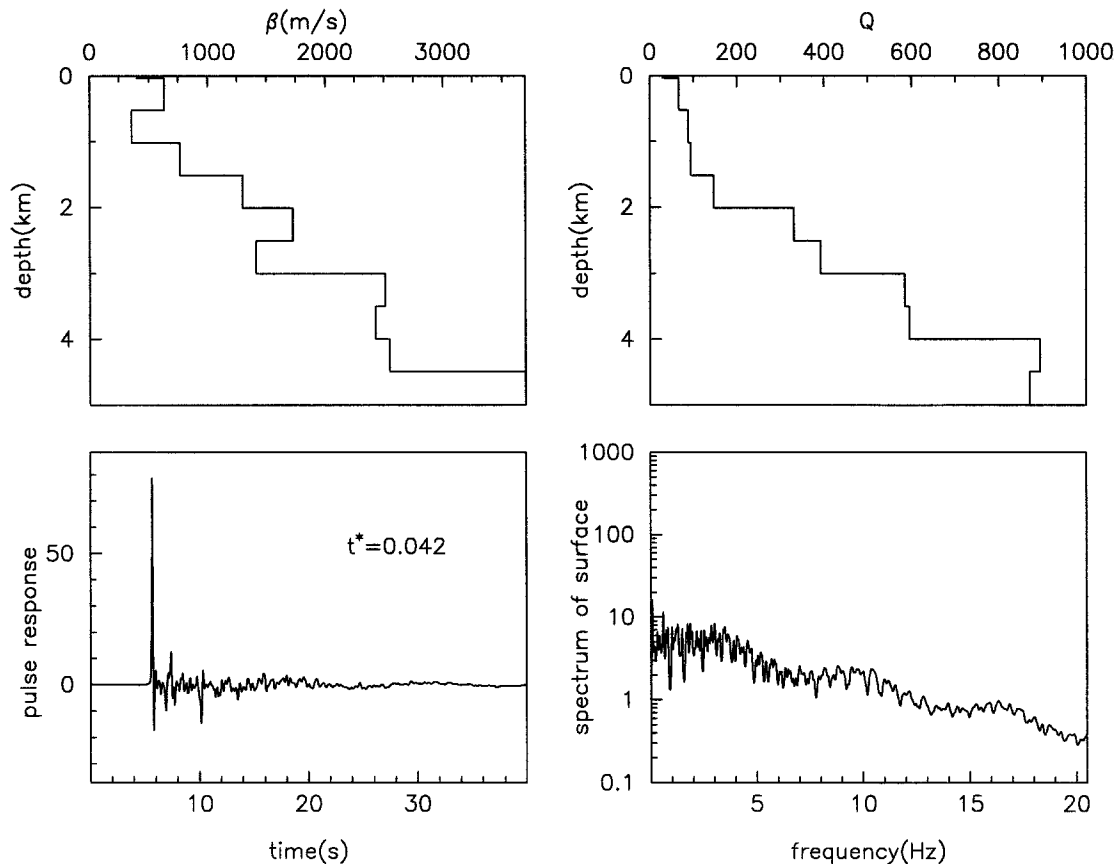


Figure 7. An example of a velocity and  $Q$  model with randomized properties and low-velocity layers, together with the seismogram and Fourier spectrum, presented with the same format as Figure 6. The velocity and  $Q$  models begin with a 10-layer representation, for the depth range between 30 m and 5 km, of one of the smooth models in the class of models described in the caption to Figure 6. Velocity and  $Q$  were chosen at random from a uniform distribution over a range of  $\pm 30\%$  relative to the velocity and  $Q$  in the smooth model at the center of each layer. There is no correlation between the deviation of velocity and  $Q$  from the smooth model.

site classes for hard rock, firm rock, gravel soils to soft rock, stiff clays and sandy soils, and soft soils, respectively. The SMI and the peak amplitude increase as the velocity of the surface layer decreases. This is consistent with regressions, such as Boore *et al.* (1993, 1994), that predict larger motions on softer materials. What is also conspicuous is that, over the range of  $t^*$  covered in this figure, the influence of attenuation in the underlying layers is just as strong a factor. Sites that are in different site classes based on their shallow velocity structures can have the same RMS and peak amplitudes if the deeper attenuation properties compensate. Since we believe the range of  $t^*$  covered on this figure is representative of the range found in the field, we conclude that the influence of the surface layer on ground motions is on the same order as that of attenuation in the underlying layers. There is no reason that either one can be neglected.

These results suggest that an important contribution to the scatter in the prediction of ground motions, in regressions that use a site classification based on surficial velocity, could come from the attenuation properties in underlying layers.

Still, these regressions do find a correlation between near-surface velocity and amplitude, which could result from a correlation between  $t^*$  and the near-surface velocity. Figure 9 suggests that a site classification that uses  $t^*$  could allow prediction of peak and RMS accelerations with greater accuracy than site classifications that do not use  $t^*$ . To apply this, we need a way to measure  $t^*$ , and we need to associate typical values of  $t^*$  with each site category.

The first question is if there is a practical way to evaluate  $t^*$ . Anderson and Hough (1984) observed that at high frequencies,  $f$ , the spectrum of  $S$ -wave accelerations is characterized by a trend of exponential decay,  $e^{-\pi\kappa f}$ . The spectral decay parameter,  $\kappa$ , is an empirical parameter that can be easily measured from the spectra of seismograms of large or small earthquakes. Several subsequent articles (e.g., Anderson, 1986; Hough *et al.*, 1988; Hough and Anderson, 1988) suggest that phenomena associated with attenuation give the most reasonable physical explanation for the magnitude and behavior of  $\kappa$ . Under certain assumptions,  $\kappa$  is identical to  $t^*$ : (1) when the earthquake source spectrum is flat to accel-

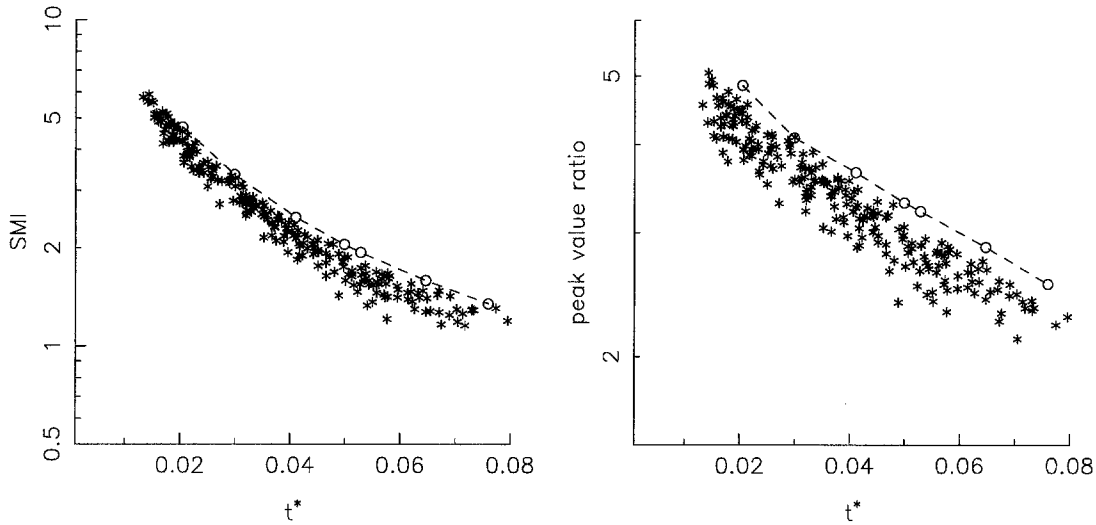


Figure 8. SMI and peak amplitude ratios, as a function of  $t^*$ , for a series of models such as those in Figures 6 and 7. The open circles, connected by the dashed lines, result from the monotonic models in the class described in Figure 6. Output of models of the type shown in Figure 7 are plotted with asterisks. For these, several members of the class are used as starting models to achieve a full range of  $t^*$  shown here. Models with monotonic increases of velocity with depth are an upper bound on the scatter in the data.

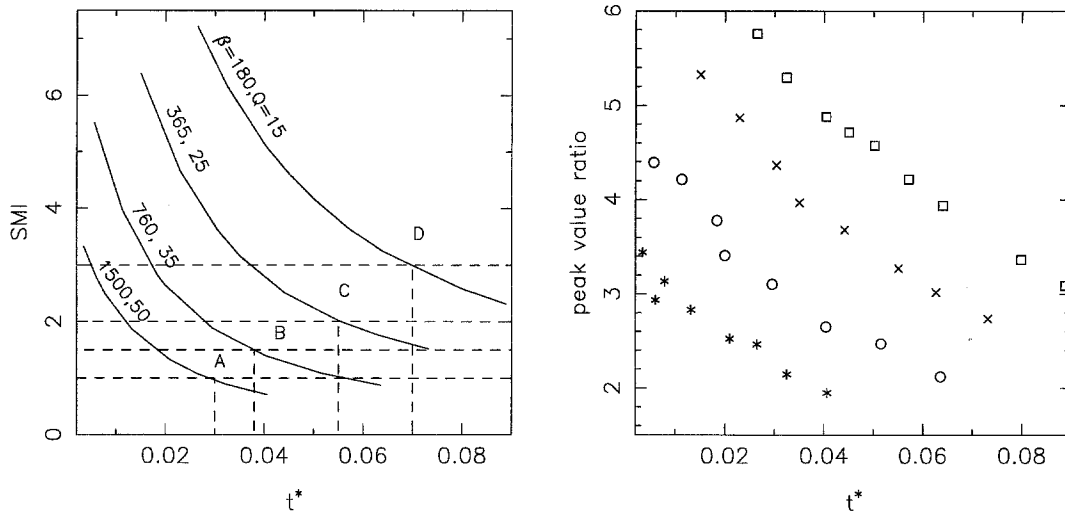


Figure 9. SMI and peak amplitude ratios for models with monotonic increases of velocity with depth, as a function of  $t^*$ . Curves correspond to different velocities in the upper 30 m. Site classification schemes that use only velocity can have overlapping SMI and peak amplitude ranges.

eration at high frequencies, (2) when  $Q$  is independent of frequency, (3) when site resonances do not severely distort the shape of the spectrum over the frequency band where  $\kappa$  is measured, and (4) where the spectral falloff is predominantly that of the direct wave. The first two assumptions are matched by our numerical experiments. We test assumptions 3 and 4 by examining the relation between  $\kappa$  and  $t^*$  for all of our numerical models. The parameter  $\kappa$  is found by a linear regression on the spectrum. The results are shown in

Figure 10, which shows that  $t^*$  is nearly equal to  $\kappa$ . Since the first two assumptions are at least rather widely used, Figure 10 suggests that  $\kappa$  can substitute for  $t^*$  in practical use. This would be consistent with the results in Figure 2, where the station with the lower value of  $\kappa$  (ASH) has a larger peak acceleration (by about 35%).

The range of  $t^*$  shown in Figure 9 matches the observed range of  $\kappa$  in California (Anderson and Hough, 1984; Hough *et al.*, 1988; Anderson, 1991). However, we need to asso-

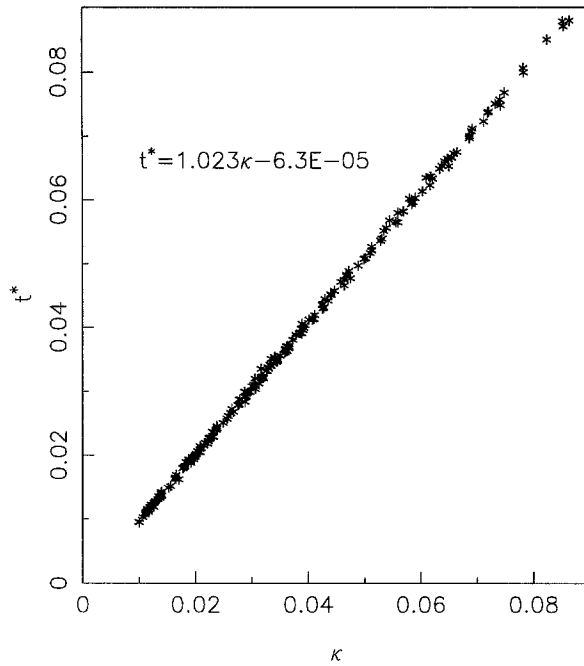


Figure 10. Relationship between  $t^*$  and  $\kappa$ .

ciate a typical value of  $t^*$  to each site class boundary in order to develop an improved site classification system. Based on observed values of  $\kappa$  in California and additional preliminary results for the Northridge earthquake (Lee and Anderson, 1996), we used the preliminary values given in Table 1. Given these, we can define site classes A, B, C, and D by common levels of SMI, as given in Table 1. Figure 11 shows contours of SMI as a function of  $t^*$  and  $\beta$  for the numerical experiments in this study.

We test this site classification concept using 3D simulations to include the additional effects of  $P$  waves, conversion of phases, nonvertical incidence, and presence of surface waves. We utilize the composite source model (Zeng *et al.*, 1994) to generate the seismograms. The test earthquake has a moment magnitude 6.0, with hypocenter 13.0 km in depth. The epicentral distance is 50 km. Similar to 1D calculations, we fix the properties of the upper 30 m to the boundaries for site classification and vary the properties below to 5 km in depth. For each model, we calculate the Green's function and convolve it with a source function to generate the synthetic seismograms. Since the horizontal components are of greatest concern, we present the average Arias intensity and peak value (neither normalized in this case) from the two horizontal components as a function of  $\kappa$  in Figure 12. The range of Arias intensity in Figure 12 is consistent with a regression and the range of observations given by Wilson (1993). The frequency band we use to calculate  $\kappa$  is from 2.0 to 20.0 Hz. The results show the same trends as those obtained from 1D numerical models.

### Discussion and Conclusion

We have examined the influences of both the surficial properties and the underlying geology on two characteristics

Table 1

Preliminary values of  $t^*$  associated with transition velocities between site categories, and preliminary estimates of increase in SMI over that on a very hard rock outcrop, assuming linear soil behavior

Boundary	$\beta$ (m/sec)	$t^*$ (sec)	SMI
A <sub>0</sub> -A	1500	0.030	1
A-B	760	0.040	1.5
B-C	365	0.055	2
C-D	180	0.070	3

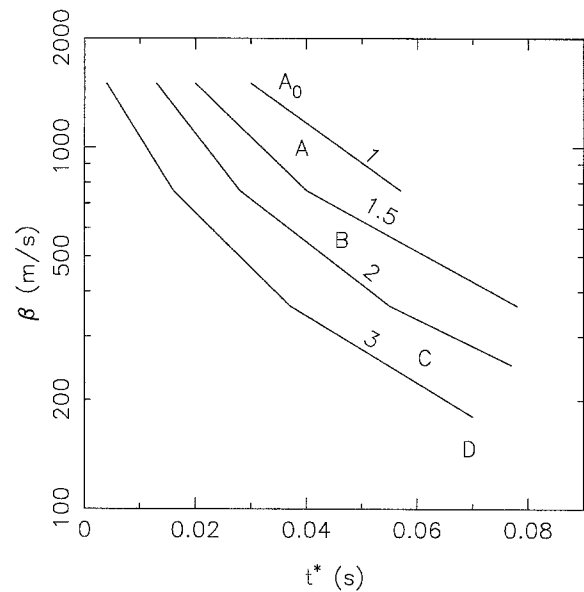


Figure 11. Contours of SMI as a function of  $t^*$  and average velocity in the upper 30 m. Based on the model in this article, this could be used to refine site classifications based on near-surface velocity along. Boundaries between different site categories are based on a preliminary association between velocity and average value of  $\kappa$  (Table 1).

of ground motions: peak amplitudes and SMI. SMI is simply the term used in this article for the integrated squared amplitude of the seismogram, normalized to equal unity at the surface of a uniform half-space representing a rock outcrop. Our numerical results suggest that, while the surficial geology has a greater influence on ground motions than might be expected based on its thickness alone, criteria for site classification based on near-surface properties alone are incomplete. Resonant frequencies depend on the depth of the deposit, of course, but the SMI and peak amplitudes depend on a bandwidth that is broader than these resonances. Extending the conclusions of Day (1996), the SMI and peak amplitudes depend only weakly on the velocity structure of the intermediate layers even in an attenuating medium. The attenuation structure in the deeper deposits is, however, a critical factor that seems to have an influence comparable in strength to the velocity in the upper 30 m but has been over-

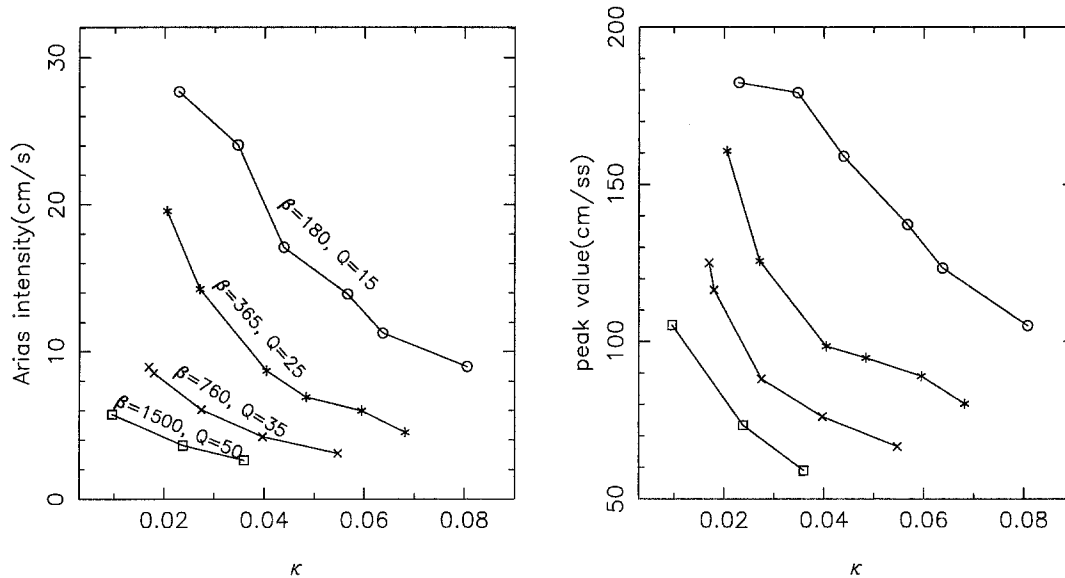


Figure 12. Modified Arias intensity (integral of acceleration squared) and peak accelerations (from horizontal components) for a series of synthetic seismograms generated with a three-dimensional simulation method (see text). All seismograms are from a source with a moment magnitude of 6.0 at a distance of 50 km. Lines connect calculations with common velocity in the upper 30 m. Differences in  $\kappa$  result from differing velocity and  $Q$  models between 30 m and 5 km in depth.

looked in the past to some extent. We find that the SMI and peak amplitudes at the surface should depend exponentially on  $t^*$ , which depends primarily on  $Q$  in intermediate layers. We suggest that  $\kappa$  is a useful parameter to characterize attenuation properties of the underlying structures, since it can be measured empirically and, under the assumptions used in this article, is correlated to  $t^*$ . These results thus predict that the velocity in the upper 30 m, the observed value of  $\kappa$ , and observed resonant frequencies might be sufficient to characterize a site in regions where 1D models are appropriate.

Our results are based on a quite idealized, one-dimensional flat model. Nonlinear site response to the incident ground motion also is not included in our models. However, our preliminary calculations indicate that the results will generalize to three-dimensional situations, and thus the results should have general significance.

### Acknowledgments

We thank Leif Wennerberg for helpful information on the examples shown in Figure 2. We appreciate helpful reviews of the manuscript by W. Joyner and M. Chapman. This research was supported by the Southern California Earthquake Center (SCEC Contribution Number 224).

### References

Anderson, J. G. (1986). Implication of attenuation for studies of the earthquake source, *Earthquake Source Mechanics, Geophysical Monograph 37, (Maurice Ewing Series 6)*, American Geophysical Union, Washington, D.C. 311–318.W.

Anderson, J. G. (1991). A preliminary descriptive model for the distance

dependence of the spectral decay parameter in southern California, *Bull. Seism. Soc. Am.* **81**, 2186–2193.

Anderson, J. G. and S. Hough (1984). A model for the shape of the Fourier amplitude spectrum of acceleration at high frequencies, *Bull. Seism. Soc. Am.* **74**, 1969–1994.

Arias, A. (1970). A measure of earthquake intensity, in *Seismic Design of Nuclear Power Plants*, R. J. Hansen (Editor), M. I. T. Press, Cambridge, Massachusetts, pp. 438–483.

Boore, D. M., W. B. Joyner, and T. E. Fumal (1993). Estimation of response spectra and peak accelerations from western United States earthquakes: an interim report, *U.S. Geol. Surv. Open-File Rep. 93-509*, 72 pp.

Boore, D. M., W. B. Joyner, and T. E. Fumal (1994). Estimation of response spectra and peak accelerations from western United States earthquakes: an interim report, Part 2, *U.S. Geol. Surv. Open-File Rep. 94-127*, 40 pp.

Borcherdt, R. D. (1992). Simplified site classes and empirical amplification factors for site-dependent code provisions, in *Proc. NCEER, SEAOC, BSSC Workshop on Site Response during Earthquakes and Seismic Code Provisions*, November 18–20, University of Southern California, Los Angeles, California.

Borcherdt, R. D. (1994). Estimates of site-dependent response spectra for design (methodology and justification), *Earthquake Spectra* **10**, 617–653.

Brune, J. N. (1970). Tectonic stress and spectra of seismic shear waves from earthquakes, *J. Geophys. Res.* **75**, 4997–5009.

Day, S. M. (1996). RMS response of a one-dimensional half-space to SH, *Bull. Seism. Soc. Am.* **86**, 363–370.

Fletcher, J. B., T. Fumal, H.-P. Liu, and L. C. Haar (1990). Near-surface velocities and attenuation at two boreholes near Anza, California, from logging data, *Bull. Seism. Soc. Am.* **80**, 807–831.

Gibbs, J. F. and E. F. Roth (1989). Seismic velocities and attenuation from borehole measurements near the Parkfield prediction zone, central California, *Earthquake Spectra* **5**, 531–537.

Gibbs, J. F., D. M. Boore, W. B. Joyner, and T. E. Fumal (1994). The

- attenuation of seismic shear waves in Quaternary alluvium in Santa Clara Valley, California, *Bull. Seism. Soc. Am.* **84**, 76–90.
- Hanks, T. C. (1979).  $b$  values and  $\omega^{-\gamma}$  seismic source models: implications for tectonic stress variations along active crustal fault zones and the estimation of high-frequency strong ground motion, *J. Geophys. Res.* **84**, 2235–2242.
- Hanks, T. C. and R. K. McGuire (1981). The character of high-frequency strong ground motion, *Bull. Seism. Soc. Am.* **71**, 2071–2095.
- Hauksson, E., T. Teng, and T. L. Henyey (1987). Results from a 1500 m deep, three-level downhole seismometer array: site response, low  $Q$  values, and  $f_{max}$ , *Bull. Seism. Soc. Am.* **77**, 1883–1904.
- Hough, S. E. and J. G. Anderson (1988). High-frequency spectra observed at Anza, California: implications for  $Q$  structure, *Bull. Seism. Soc. Am.* **78**, 692–707.
- Hough, S. E., J. G. Anderson, J. Brune, F. Vernon III, J. Berger, J. Fletcher, L. Haar, T. Hanks, and L. Baker (1988). Attenuation near Anza, California, *Bull. Seism. Soc. Am.* **78**, 672–691.
- Joyner, W. B., R. E. Warrick, and T. E. Fumal (1981). The effect of Quaternary alluvium on strong ground motion in the Coyote Lake, California earthquake of 1979, *Bull. Seism. Soc. Am.* **71**, 1333–1349.
- Lee, Y. and J. G. Anderson (1996). Typical values of the spectral decay parameter, 'kappa' (in preparation).
- Luco, J. E. and R. J. Apsel (1983). On the Green's function for a layered half space, Part I, *Bull. Seism. Soc. Am.* **73**, 909–929.
- Martin, G. R. and R. Dobry (1994). Earthquake site response and seismic code provisions, *NCEER Bull.* **8**, 1–6.
- Richards, P. G. and W. Menke (1983). The apparent attenuation of a scattering medium, *Bull. Seism. Soc. Am.* **73**, 1005–1021.
- Sanchez-Sesma, F. J., E. Faccioli, and R. Fregonese (1986). An index for measuring the effects of topography on seismic ground motion intensity, *Earthquake Eng. Struct. Dyn.* **14**, 719–731.
- Thiel Jr., C. C. and J. F. Schneider (1993). Investigations of thirty-three Loma Prieta earthquake strong motion recording sites, Final Report of Project Sponsored by the Building Contractors Society of Japan and the Electric Power Research Institute, California Universities for Research in Earthquake Engineering (CUREe), Dept. of Civil Engineering, Stanford Univ., Stanford, California.
- Wilson, R. C. (1993). Relation of Arias intensity to magnitude and distance in California, *U.S. Geol. Surv. Open-File Rept.* 93–556, Menlo Park, California.
- Yu, G. (1994). Some aspects of earthquake seismology: slip partitioning along major convergent plate boundaries; composite source model for estimation of strong motion; and nonlinear soil response modeling, *Ph.D. Thesis*, University of Nevada, Reno, 144 pp.
- Zeng, Y., K. Aki, and T.-L. Teng (1993). Mapping of the high-frequency source radiation for the Loma Prieta earthquake, California, *J. Geophys. Res.* **98**, 11981–11993.
- Zeng, Y., J. G. Anderson, and G. Yu (1994). A composite source model for computing realistic synthetic strong ground motions, *Geophys. Res. Lett.* **21**, 725–728.
- Seismological Laboratory and Department of Geological Sciences  
Mackay School of Mines  
University of Nevada  
Reno, Nevada 89557  
(J.G.A., Y.L.)
- Seismological Laboratory  
Mackay School of Mines  
University of Nevada  
Reno, Nevada 89557  
(Y.Z.)
- Department of Geological Sciences  
San Diego State University  
San Diego, California 92182  
(S.D.)

Manuscript received 29 August 1995.